

# Accurate color synthesis of three-dimensional objects in an image

John H. Xin and Hui-Liang Shen

*Institute of Textiles and Clothing, The Hong Kong Polytechnic University, Hong Kong, China*

Received June 15, 2003; revised manuscript received December 5, 2003; accepted December 10, 2003

Our study deals with color synthesis of a three-dimensional object in an image; i.e., given a single image, a target color can be accurately mapped onto the object such that the color appearance of the synthesized object closely resembles that of the actual one. As it is almost impossible to acquire the complete geometric description of the surfaces of an object in an image, this study attempted to recover the implicit description of geometry for the color synthesis. The description was obtained from either a series of spectral reflectances or the RGB signals at different surface positions on the basis of the dichromatic reflection model. The experimental results showed that this implicit image-based representation is related to the object geometry and is sufficient for accurate color synthesis of three-dimensional objects in an image. The method established is applicable to the color synthesis of both rigid and deformable objects and should contribute to color fidelity in virtual design, manufacturing, and retailing. © 2004 Optical Society of America

*OCIS codes:* 330.1690, 330.1720, 100.3020.

## 1. INTRODUCTION

The perception of color has been the subject of research in many disciplines, including computer graphics and computer vision. One of the major goals of computer graphics is to synthesize realistic images of scenes modeled in a computer. To create such a realistic image, a complete model or description of the reflectance is needed for each of the reflective objects in the scene. It is difficult to establish a complete representation of the reflective behavior of the surface of an object because of the complex interactions between the light and the surface, such as polarization, scattering, phosphorescence, and fluorescence. For opaque surfaces, the description of the bidirectional reflectance distribution function (BRDF) described by Nicodemus *et al.*<sup>1</sup> at each point on an object surface is needed; it is a function of four dimensions (two for incident angles and two for reflective angles). When the geometry and characteristics of the object surface are known, the empirical physics-based BRDF models can be used for color rendering.<sup>2-4</sup> Alternatively, the BRDF data can also be measured experimentally with custom-built equipment.<sup>5,6</sup> For the convenient use of BRDF data, some researchers have built BRDF databases for some real-world surfaces, such as wood, paper, and polyester.<sup>7,8</sup> Owing to problems with the positioning precision of the light source and the imaging device, and with the irregularity of the surface geometry, it is quite difficult to measure BRDF data accurately even with careful design of the measurement system.<sup>6,7</sup>

In contrast to computer graphics, the physics-based approach in computer vision is aimed at recovering the surface orientation from gray or color images, or “shape from X” (X denotes shading, shadow, highlight, etc.).<sup>9</sup> “Shape from X” is an ill-posed problem and is currently far from being satisfactorily solved. Practically, constraints must be adopted to reach reasonable solutions to the problem of shape description. In exploiting the complex interaction

between the illumination and the surface, the experiential dichromatic reflection model introduced by Shafer was the first realistic color reflection model used in computer vision.<sup>10</sup> This model has been studied and extended by others and works well for a large class of inhomogeneous materials such as plastic, leaf, wood, and ceramic.<sup>11-13</sup> However, Tominaga found that the standard model was inadequate for the description of some materials such as satin and silk fabrics, and he therefore proposed an extension of the dichromatic reflection model so that these materials can also be described.<sup>13</sup> On the basis of the extended model, Tominaga further presented a method for the rendering of three-dimensional (3-D) objects by using the measured reflectance.<sup>14</sup> In his work, the geometric weighting for body reflectance and surface reflectance were specified according to the models developed by Phong<sup>2</sup> and Torrance and Sparrow<sup>4</sup> for different categories of materials. Recently, Xin and Shen also introduced an image-based method for the accurate rendering of texture images by using dichromatic reflection model.<sup>15</sup>

The objective of the current study was to map any color defined by a set of tristimulus values or spectral reflectance to an object under a given illumination such that the appearance of the synthesized image is perceptually very similar to that of the actual scene. More precisely, given an image of an object with intrinsic color  $R(\lambda)$ , where  $\lambda$  is wavelength, viewed under an illumination with spectral power distribution  $L(\lambda)$ , the objective is to generate a new image of the same object but with different color  $R'(\lambda)$  under a different illumination  $L'(\lambda)$  from the same viewpoint. The algorithm is image based and does not require the explicit geometry of 3-D objects; thus it is computationally effective. The potential applications of the proposed algorithm are image-based 3-D object simulation and visualization, with emphasis on color fidelity. A similar method called color transfer was re-

cently conducted by Reihard *et al.*<sup>16</sup>; the procedure is to change the colors of an original image by using the colors of another image on the basis of color statistical information. The color transfer method performs well for scene modification, but the color accuracy has not been adequately addressed. In this study we simplify the generic BRDF by assuming parallel lighting conditions and fixed imaging geometry. The implicit geometric description of the objects was recovered from an image by using the dichromatic reflection model. Two very different materials, namely, plastic and textile fabric, were used in the experiment. The main difference between the model developed in this study and the one in Tominaga's study<sup>14</sup> is that the former calculates the geometric information directly from an image whereas the latter uses explicitly specified geometric information. Therefore the model developed in this study has the advantage of rendering an object without the knowledge of explicit geometry. In previous studies of image-based color modification based on the dichromatic reflection model,<sup>17,18</sup> the problem of whether the geometric information obtained was accurate enough for the color synthesis of 3-D objects was not addressed. We investigated this problem in our study by using color difference evaluation and statistical analysis.

## 2. BIDIRECTIONAL REFLECTANCE DISTRIBUTION FUNCTION AND IMAGING GEOMETRY

The BRDF  $f_r$  is a generic form for light reflection modeling in most of the applications of both computer graphics and computer vision. It is defined as the ratio of the reflected radiance  $dL_r$ , in the direction of viewing to the irradiance  $dE_i$ , in the direction of the incident light.<sup>12,19</sup> To study the spectral reflection behavior, we can extend the BRDF by including the parameter of wavelength,

$$f_r(\theta_i, \phi_i; \theta_r, \phi_r; \lambda) = \frac{dL_r(\theta_i, \phi_i; \theta_r, \phi_r; \lambda; E_i)}{dE_i(\theta_i, \phi_i; \lambda)}, \quad (1)$$

where  $\lambda$  denotes wavelength in the visible spectrum,  $(\theta_i, \phi_i)$  and  $(\theta_r, \phi_r)$  are the angles of incident and reflected light shown in Fig. 1, and  $E_i$  is the irradiance at a point on the surface.

Figure 1 describes the geometry for BRDF definition. A surface-specific coordinate system is erected with one axis along the local normal to the surface,  $Z$ , and another

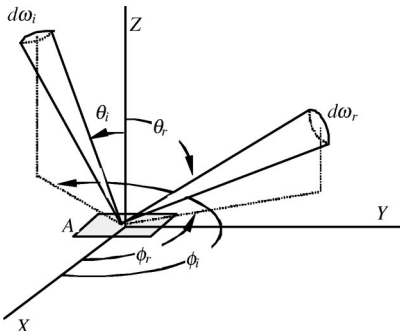


Fig. 1. Geometry of incident and reflected light defined in the BRDF.

reference axis,  $X$ , is defined arbitrarily in the local tangent plane. The directions of the incident and the reflected light are specified by the polar angle  $\theta$  measured from the local normal and the azimuth angle  $\phi$ , respectively, measured counterclockwise from the  $X$  axis of the surface. In general, incident flux may come from different locations of light sources, such that the incident spectral radiance  $L_i(\theta_i, \phi_i)$  is a function of direction. The reflected spectral radiance can be calculated by the double integration in the hemisphere above the object surface<sup>19</sup>:

$$L_r(\theta_r, \phi_r; \lambda) = \int_{-\pi}^{\pi} \int_0^{\pi/2} f_r(\theta_i, \phi_i; \theta_r, \phi_r; \lambda) L_i(\theta_i, \phi_i; \lambda) \cos \theta_i \sin \theta_i d\theta_i d\phi_i. \quad (2)$$

The polar angle  $\theta_i$  is from 0 to  $\pi/2$ , and  $\phi_i$  is from  $-\pi$  to  $\pi$ . We make the assumption that the light is isotropic within the range of  $\phi_i$  for the small surface  $A$  in Fig. 1 and is incident from the direction  $\theta$ ; then the incident spectral radiance can be represented by

$$L_i(\theta_i, \phi_i; \lambda) = L(\lambda) \delta(\theta_i - \theta), \quad (3)$$

where  $L(\lambda)$  is the incident spectral radiance, and the Dirac delta function  $\delta(\theta_i - \theta)$  is defined as

$$\delta(\theta_i - \theta) = \begin{cases} 1, & \theta_i = \theta \\ 0, & \theta_i \neq \theta \end{cases}. \quad (4)$$

The assumption of parallel (or directional) lighting is not stringent and can be achieved with good approximation when the object is relatively far from the light source. Substituting Eq. (3) into Eq. (2) gives the reflected spectral radiance as

$$L_r(\theta_r, \phi_r; \lambda) = \frac{1}{2} L(\lambda) \cos 2\theta \times \int_{-\pi}^{\pi} f_r(\theta, \phi_i; \theta_r, \phi_r; \lambda) d\phi_i. \quad (5)$$

If the lighting geometry has no significant change in the imaging process, the integration of the BRDF can be written by using its average form over the azimuth incident angle as

$$\bar{f}_r(\theta_r, \phi_r; \lambda) = \frac{1}{2} \cos 2\theta \int_{-\pi}^{\pi} f_r(\theta, \phi_i; \theta_r, \phi_r; \lambda) d\phi_i. \quad (6)$$

Accordingly, the reflected spectral radiance is given by

$$L_r(\theta_r, \phi_r; \lambda) = L(\lambda) \bar{f}_r(\theta_r, \phi_r; \lambda). \quad (7)$$

If the distance between the object and the imaging device is much larger than the focal length and the diameter of the entrance aperture of the imaging system, the image spectral irradiance  $E_p$  is proportional to scene spectral radiance  $L_r$ :

$$E_p(\lambda) = c(\alpha) L(\lambda) \bar{f}_r(\theta_r, \phi_r; \lambda), \quad (8)$$

where  $c(\alpha)$  is a factor relative to  $\alpha$ , the angle between reflected light and the optical axis of the imaging device.

In most cases, a camera is used as the imaging device. Therefore the camera output signal  $V_k$  of the  $k$ th sensor is

$$V_k = \int E_p(\lambda) S_k(\lambda) d\lambda = c(\alpha) \int L(\lambda) S_k(\lambda) \bar{f}_r(\theta_r, \phi_r; \lambda) d\lambda. \quad (9)$$

In Eq. (9),  $S_k(\lambda)$  represents the spectral sensitivity function of the  $k$ th sensor (e.g., red, green, blue, or equivalently 1, 2, 3) of the camera. The sensitivity  $S_k(\lambda)$  could either be measured or be calculated by using the constrained least-squares method.<sup>20</sup> Equation (9) assumes that the camera behaves in a linear fashion, i.e., that the output signal of the camera is proportional to the amount of light that enters the camera at a particular pixel position. When the linearity of the camera does not strictly hold, some strategy may be employed to correct the nonlinearity.<sup>20</sup> In this study, however, the explicit expression of the sensitivity is not necessary, and the camera is assumed to be approximately linear.

For simplicity in denotation, let  $x$  represent the reflection geometry  $(\theta_r, \phi_r)$  and  $R(\lambda)$  denote the spectral reflectance at position  $x$ ; that is,

$$R(x; \lambda) \equiv \bar{f}_r(\theta_r, \phi_r; \lambda). \quad (10)$$

Accordingly, the linear output of the camera becomes

$$V_k^x = c(\alpha^x) \int L(\lambda) S_k(\lambda) R(x; \lambda) d\lambda, \quad (11)$$

where  $\alpha^x$  denotes the angle relating to geometric position  $x$ . When the illumination is not uniform for the whole object surface, we can regard  $L(\lambda)$  as the average spectral power distribution, and the variation of illumination intensity at position  $x$  could be incorporated into the factor  $c(\alpha^x)$ . It is also worth noting that in Eq. (11) the factors  $x$  and  $\alpha^x$  are important in deciding the geometric relationships among different positions. The light source  $L(\lambda)$  and the spectral sensitivity  $S_k(\lambda)$ , however, are less important, because they are fixed in the imaging system. The effect of these factors will be further investigated in the following section.

### 3. RECOVERY OF GEOMETRY FROM REFLECTANCE AND COLOR

Figure 2 is a schematic diagram of the interaction of light and an object surface. When a ray of light strikes the surface of an inhomogeneous material, part of it is re-

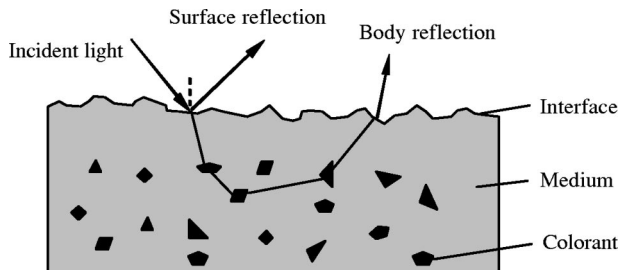


Fig. 2. Reflection from an inhomogeneous surface with two components: surface reflection and body reflection (After Fig. 1 in Ref. 10).

flected from the interface between the object and the air immediately because of the difference in the refractive indices of the object and the air. This part of light is called surface reflection (or specular reflection). The surface reflection is dependent on the orientation of the local surface, which varies along the interface. When the surface is smooth, the surface reflection is very directional, and when the surface has some degree of roughness, the light rays are scattered to some extent around the angle of perfect mirror reflection. In addition to the surface reflection, part of the light penetrates the interface and enters the body of the object, where it keeps hitting the colorants and is scattered by the colorants. The colorants and the medium also absorb part of the light. Part of the scattering light arrives back at the object surface and re-enters the air. This part of light has been selectively absorbed by the colorants and the medium. It is called body reflection (or diffuse reflection). The dichromatic reflection model can be applied to a variety of materials, including plastic, wood, ceramic, and other opaque nonconductors with uniform pigmentation. However, the dichromatic reflection model may fail to describe other materials with nonneutral surface reflections such as coated glasses, iridescent surfaces, metals, and silk fabrics. As a consequence, the algorithm discussed in the following cannot be applied to those materials.

It is assumed in the standard dichromatic reflection model that the surface reflection and the body reflection can be approximately decomposed into two independent components, i.e., spectral and geometric ones:

$$R(x; \lambda) \approx g_b(x) R_b(\lambda) + g_s(x) R_s(\lambda), \quad (12)$$

where  $g_b(x)$  and  $g_s(x)$  are the geometric factors of the body reflectance and the surface reflectance at position  $x$ , and  $R_b(\lambda)$  and  $R_s(\lambda)$  are the wavelength composition of the body reflectance and the surface reflectance, respectively. Since the spectral power distribution of the surface reflection is very similar to that of the incident light,<sup>10</sup> relation (12) can be simplified as

$$R(x; \lambda) \approx g_b(x) R_b(\lambda) + g_s(x) R_s. \quad (13)$$

Similarly, for a different position  $y$  on the same material, the reflectance is

$$R(y; \lambda) \approx g_b(y) R_b(\lambda) + g_s(y) R_s. \quad (14)$$

The reflectance  $R(x; \lambda)$  and  $R(y; \lambda)$  can be linearly related by eliminating the term  $R_b(\lambda)$  in relations (13) and (14):

$$R(y; \lambda) = aR(x; \lambda) + b + \epsilon(\lambda), \quad (15)$$

where  $\epsilon(\lambda)$  is a random error, and  $(a, b)$  is the geometric coefficient pair determined by the geometric factors  $g_s(\cdot)$  and  $g_b(\cdot)$ :

$$a = \frac{g_b(y)}{g_b(x)}, \quad (16)$$

$$b = R_s \left[ g_s(y) - \frac{g_b(y)}{g_b(x)} g_s(x) \right]. \quad (17)$$

The most straightforward method for solving Eq. (15) was considered to be the conventional least-squares method.

This method treats the reflectance at each wavelength equally. However, the sensitivity of an imaging system, whether it be the human eye or a CCD camera, is different at different wavelengths of the visible spectrum, with low sensitivity at the two extremes of the spectrum and much higher sensitivity at the center of the spectrum. Therefore in this study it was preferred to solve Eq. (15) by minimizing

$$\int w(\lambda)[R(y; \lambda) - R^*(y; \lambda)]^2 d\lambda, \quad (18)$$

where  $R^*(y; \lambda)$  is the solved reflectance at position  $y$ , and  $w(\lambda)$  is the color-matching function of the sensitivity of the camera (or the human eye). The recovered coefficients  $a$  and  $b$  describe the geometric relationship between body and surface reflections, respectively, at different positions. If the recovered  $(a, b)$  is accurate enough, it can then be used to calculate the reflectance  $R'(y; \lambda)$  at position  $y$  together with the use of the target reflectance  $R'(x; \lambda)$  at position  $x$ . Figure 3 shows how the coefficient pair  $(a, b)$  are related to the geometry and how they are used for color synthesis.

As mentioned in Section 1, traditional scene rendering is based on the shape information of objects, which is commonly measured through careful design of the experimental setup and use of special instruments such as the goniospectrometer. However, despite their high costs, these instruments may not be suitable for measuring the surface geometry of deformable objects such as those made of cloth. From Eqs. (15)–(17), it is quite clear that the geometric coefficients  $(a, b)$  record the relative geometric information at position  $y$  with respect to position  $x$ . Although the dichromatic reflection model has been intensively investigated in the literature of computer vision, to our knowledge the accuracy of the geometric coefficients has never been adequately addressed.

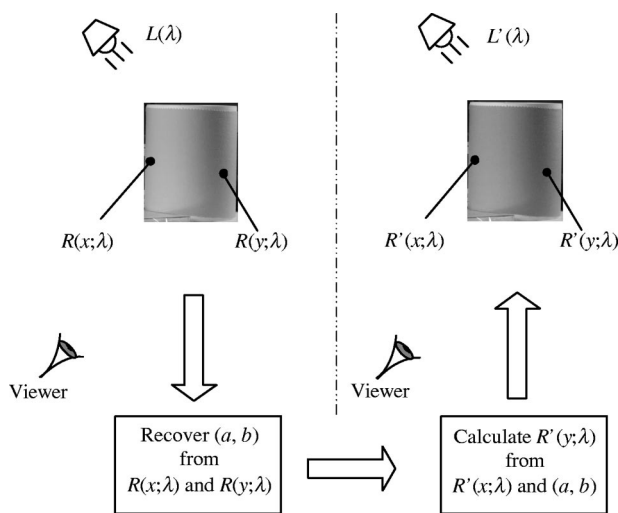


Fig. 3. Relationship between coefficient pair  $(a, b)$  and surface reflectance at different geometric positions. First, the geometric coefficient pair  $(a, b)$  can be recovered from the reflectance data at different positions (denoted  $y$ ) with respect to a reference position  $x$  (left-hand part), and then  $(a, b)$  can be used to synthesize new colors for a 3-D object (right-hand part).

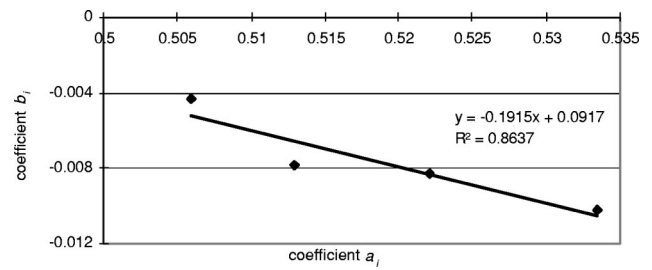


Fig. 4. Distribution of  $(a_i, b_i)$  for a material with mainly body reflection.

Assume that there are  $N$  objects of the same material and shape but different colors. Then, for the  $i$ th object, the geometric coefficients  $(a_i, b_i)$  can be calculated as

$$R^i(y; \lambda) = a_i R^i(x; \lambda) + b_i + \epsilon^i(\lambda), \quad (19)$$

where  $i = 1 \dots N$ . If coefficients  $(a_i, b_i)$  accurately record the geometric information of object surface, then, for an object with the same shape but different color whose reflectance at position  $x$  is  $R^a(x; \lambda)$ , the reflectance at position  $y$  can be calculated from any known  $(a_i, b_i)$ :

$$R^a(y; \lambda) = a_i R^a(x; \lambda) + b_i + \epsilon_i^a(\lambda) \quad \text{for } i = 1 \dots N, \quad (20)$$

where  $\epsilon_i^a(\lambda)$  is the residual spectral error. When  $(a_i, b_i)$  accurately represent the geometry,  $\epsilon_i^a(\lambda)$  should be small enough.

It should be noted that the  $(a_i, b_i)$  solved in Eq. (19) are related to the spectral distribution of the reflectance of the  $i$ th material. So it is commonly the case that

$$(a_i, b_i) \neq (a_j, b_j) \quad \text{for } i \neq j. \quad (21)$$

Therefore it is necessary to study the description accuracy of the different geometric coefficient pairs. There are two methods for evaluating the capability of geometry representation by  $(a_i, b_i)$  pairs. The first method is to calculate the tristimulus values from reflectance by using  $(a_i, b_i)$  and then to calculate the color difference between these values and the measured color values. A low computed color difference will indicate a high accuracy of the geometric coefficient  $(a_i, b_i)$ . The second method is to investigate the distribution of the  $(a_i, b_i)$  pairs statistically.

To analyze the statistical distribution of  $(a_i, b_i)$ , we used two very different materials, i.e., plastic and fabric. The experimental setup and the measurement detail of the reflectance data will be discussed in Section 4. When there is little surface reflection, the magnitude of coefficient  $b_i$  is always significantly smaller than that of coefficient  $a_i$ , as shown in Fig. 4. Further analysis revealed that the majority of  $(a_i, b_i)$  pairs are either located in a very small region or are negatively correlated; i.e., the value of  $b_i$  is low when the value of  $a_i$  is high, and vice versa. Besides being the result of different reflectance shapes, this characteristic may also be caused by measurement noise. When there is little noise, the recovered  $(a_i, b_i)$  pairs should be very similar. On the other hand, if there is more noise, the distribution of  $(a_i, b_i)$  may be biased. However, since the calculation of  $(a_i, b_i)$  by using either the traditional or the weighted least-squares method is actually an error-minimization problem, the

combined effect of  $a_i$  and  $b_i$  should not deviate greatly from the correct values. This may be why the distributions of  $a_i$  and  $b_i$  are always negatively correlated. As a result of this characteristic of the  $(a_i, b_i)$  pairs, the difference between the calculated  $R^a(x; \lambda)$  in Eq. (20) with use of different  $(a_i, b_i)$  pairs should be relatively small, because the variation of  $a_i$  is compensated by the inverse variation of  $b_i$  to some degree. It is of interest to estimate statistically the variation of the spectral error introduced by the different geometric coefficient pairs. For simplicity, a scalable quantity  $R$  is used in the estimation instead of the vector quantity  $R^a(x; \lambda)$  in Eq. (20). The estimation of the reflectance difference caused by the variation of  $(a_i, b_i)$  pairs can then be defined as

$$E = \int_R \frac{1}{N} \sum_{i=1}^N |(\bar{a}R + \bar{b}) - (a_iR + b_i)| p(R) dR, \quad (22)$$

where  $\bar{a}$  and  $\bar{b}$  are the mean values of  $a_i$  and  $b_i$  ( $i = 1..N$ ), respectively, and  $p(R)$  is the probability of reflectance  $R$ . Equation (22) can be rewritten as

$$E = \frac{1}{N} \int_R \sum_{i=1}^N |(\bar{a} - a_i)R + (\bar{b} - b_i)| p(R) dR. \quad (23)$$

It is well known that for two variables  $\alpha_1$  and  $\alpha_2$ ,

$$|\alpha_1 + \alpha_2| \leq |\alpha_1| + |\alpha_2|, \quad (24)$$

and hence the expectation can be expressed by an inequality:

$$E \leq \frac{1}{N} \sum_{i=1}^N |\bar{a} - a_i| \int_R p(R) R dR + \frac{1}{N} \sum_{i=1}^N |\bar{b} - b_i| \int_R p(R) dR. \quad (25)$$

Assuming that the probability of the reflectance is equally likely in the range of  $[0, 1]$ , inequality (25) then becomes

$$E \leq \frac{1}{2N} \sum_{i=1}^N (|\bar{a} - a_i| + 2|\bar{b} - b_i|). \quad (26)$$

Therefore, from the distribution of  $(a_i, b_i)$  pairs, we can estimate the reflectance difference introduced by the variation of  $(a_i, b_i)$ . If the right-hand side of inequality (26) is small enough, the  $(a_i, b_i)$  pairs can be expected to be capable of recovering the geometric information of the material surface accurately.

According to Eq. (11), the output at position  $y$  can be defined as

$$V_k^y = c(\alpha^y) \int L(\lambda) S_k(\lambda) R(y; \lambda) d\lambda, \quad (27)$$

where  $\alpha^y$  is the off-axis angle at position  $y$ . Since  $R(y; \lambda)$  can be represented by  $R(x; \lambda)$  along with geometric coefficient  $(a, b)$ , Eq. (27) becomes

$$\begin{aligned} V_k^y &= c(\alpha^y) \int L(\lambda) S_k(\lambda) (aR(x; \lambda) + b) d\lambda \\ &= c(\alpha^y) \left( a \int L(\lambda) S_k(\lambda) R(x; \lambda) d\lambda \right. \\ &\quad \left. + b \int L(\lambda) S_k(\lambda) d\lambda \right) \\ &= AV_k^x + BW_k, \end{aligned} \quad (28)$$

where

$$A = \frac{c(\alpha^y)}{c(\alpha^x)} a, \quad (29)$$

$$B = c(\alpha^y) b, \quad (30)$$

$$W_k = \int L(\lambda) S_k(\lambda) d\lambda. \quad (31)$$

The geometric coefficient pair  $(A, B)$  can be calculated from  $V_k^x$  and  $V_k^y$ , and  $W_k$  is in fact the camera response of a perfect white diffuser under illuminant  $L(\lambda)$ . Since  $W_k$  is assumed to be known for a given imaging system and there are three known output pairs and two unknowns  $(A, B)$ , the problem is overdetermined. The geometric coefficient pair  $(A, B)$  in RGB color space can be calculated by the least-squares method. If we let  $\hat{V}_k^y$  be the estimation of  $V_k^y$  in the  $k$ th channel, the residual error can be calculated as

$$\epsilon_V = [(V_1^y - \hat{V}_1^y)^2 + (V_2^y - \hat{V}_2^y)^2 + (V_3^y - \hat{V}_3^y)^2]^{1/2}. \quad (32)$$

Therefore with a reference  $V_k^x$ , given a single image, the geometric coefficient pair  $(A, B)$  can be calculated by Eq. (28), and the term  $\epsilon_V$  represents the quality of the fitting result with use of the dichromatic reflection model. Since the output  $V_k^x$  is in the range of  $[0, 255]$ , similarly to inequality (26), the estimation of the quantity variation caused by different  $(A_i, B_i)$  pairs is

$$E_V \leq \frac{1}{N} \sum_{i=1}^N (128|\bar{A} - A_i| + |\bar{B} - B_i|), \quad (33)$$

when the probability of color for synthesis is assumed to be equally likely, where  $\bar{A}$  and  $\bar{B}$  are the mean values of  $A_i$  and  $B_i$  ( $i = 1..N$ ), respectively.

When the geometry can be represented by the coefficient pair  $(a, b)$  or  $(A, B)$ , the color synthesis under different illumination is quite straightforward. Let  $\tilde{L}(\lambda)$  be the spectral radiance of the new illumination; then the output quantity of the  $k$ th sensor at position  $x$  under this illumination is

$$\tilde{V}_k^x = c(\alpha^x) \int \tilde{L}(\lambda) S_k(\lambda) \tilde{R}(x; \lambda) d\lambda. \quad (34)$$

By using the geometric coefficients  $(A, B)$  calculated in a given image, we can synthesize the  $k$ th output at position  $y$  under the new illumination as

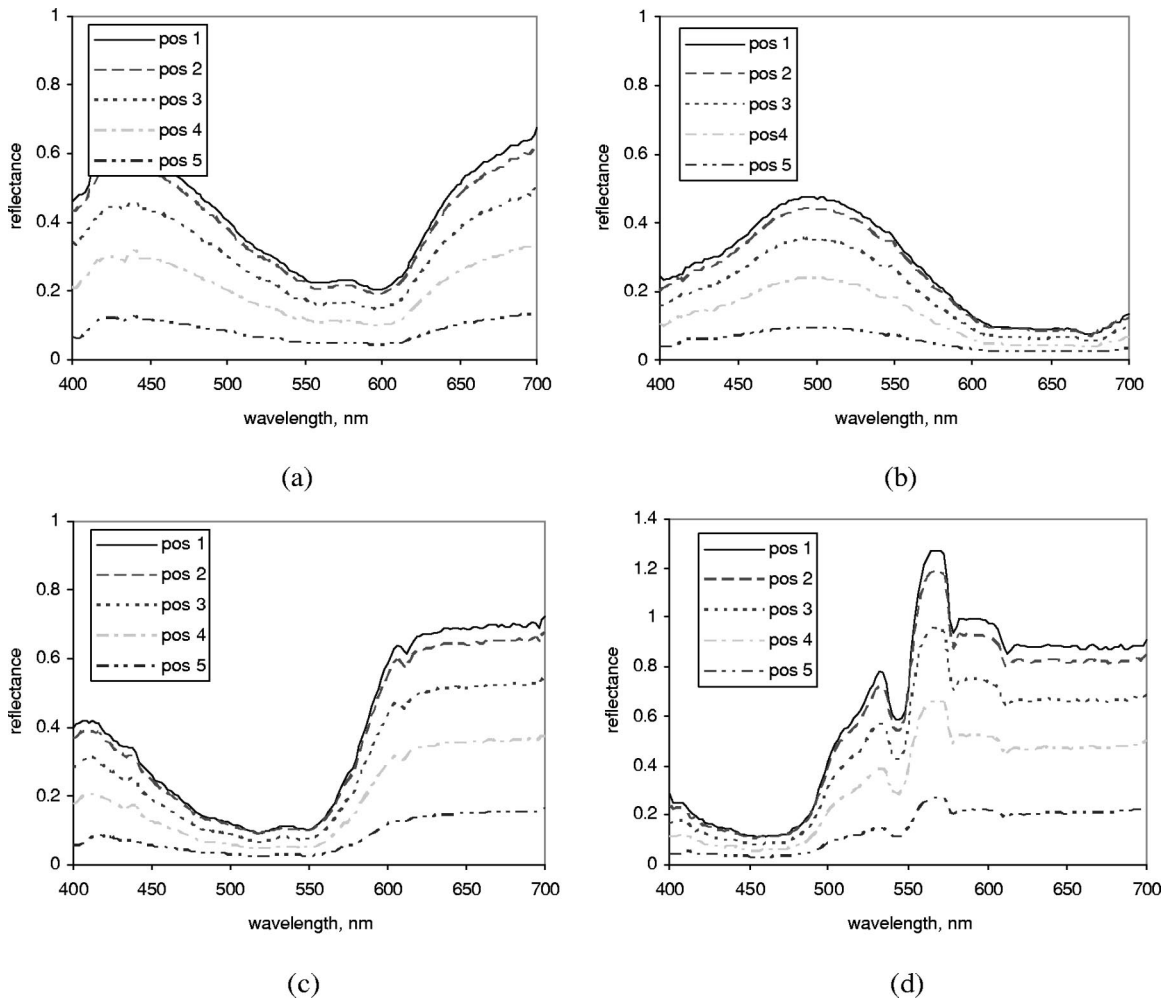


Fig. 5. Measured reflectance of four plastic cups at five different geometric positions. (a) blue cup, (b) green cup, (c) red cup, (d) yellow cup.

$$\tilde{V}_k^y = A \tilde{V}_k^x + B \frac{\int \tilde{L}(\lambda) S_k(\lambda) d\lambda}{\int L(\lambda) S_k(\lambda) d\lambda} = A \tilde{V}_k^x + B \frac{\tilde{W}_k}{W_k}, \quad (35)$$

where  $\tilde{W}_k$  is the camera response to an ideal white diffuser under illuminant  $\tilde{L}(\lambda)$ .

#### 4. EXPERIMENT AND DISCUSSION

In the experiment, two types of materials, rigid and deformable, were studied to evaluate whether the proposed method could be used satisfactorily to synthesize 3-D objects with high color fidelity. The first type of material was plastic. The objects used were four plastic cups of the same size but different colors, namely, red, green, blue, and yellow. The second type of material was polyester/cotton textile fabric, which is a deformable material. To keep the fabric in a fixed shape, the pieces were wrapped onto cylinders with the same radius and height. The objects were placed on an experiment desk, and the locations were kept fixed during the whole measurement and imaging procedure. A light source was tuned to provide nearly parallel lighting on the desk. A

perfect diffuser, a barium-sulfate-coated white reference tile, was placed in the same position so that the spectral radiance of the illumination could be measured by a spectroradiometer (Photo Research model PR704). A digital camera (Canon EOS D30) was used in the imaging system. During the measurement, the distance between the spectroradiometer and the objects was kept unchanged, and the measurements of different geometric positions on the object surface were achieved by panning and tilting the spectroradiometer.

The measurement procedure is as follows:

1. Adjust the direction of the light source so that it produces an even lighting field on the experiment desk. Warm up the light source for about an hour so that the light illumination is stable.
2. Place the barium sulfate tile on a predetermined place and measure its spectral radiance using the spectroradiometer.
3. Place an object (e.g., a red plastic cup) on the predetermined place and measure its spectral radiance. Replace the object with another object (e.g., a green plastic cup) and measure its radiance.
4. Change the measurement position on the objects, and repeat step 3 until enough data are collected.

5. Use the digital camera instead of the spectroradiometer to take images for these objects.

After the measurement, the spectral reflectance data at different geometric positions were calculated as the ratio of the spectral radiance of the object surface to that of the perfect diffuser. Figure 5 shows the reflectance data for plastic cups at five different positions on the object surface in the visible spectrum ranging from 400 to 700 nm, with intervals of 2 nm. Because the surfaces of the plastic objects were glossy, the spectral reflectance of the yellow plastic cup [Fig. 5(d)] at some positions was larger than 1.0.

We took the reflectance at the first position as the reference and calculated the geometric coefficient  $(a_i, b_i)$  at the other four positions. The distribution of the  $(a_i, b_i)$  pairs is plotted in Fig. 6. It is clear that for a particular position, the variation of the coefficient  $a_i$  is quite small. The accuracy of the  $(a_i, b_i)$  pairs can be evaluated by the color difference between the measured and the synthesized reflectance. The color differences  $\Delta E_{CMC(1:1)}^*$  (Ref. 21) for the plastic and the fabric materials are given in the Tables 1 and 2, respectively. The color difference values in the Table 1 are calculated between the reflectance of a position on the blue cup and the synthesized reflectance of the corresponding positions. Because the  $(a_1, b_1)$  are solved directly by the reflectance data of the blue cup, the color difference values of the first column in Table 1 are accordingly the lowest among all the results. The same is true in Table 2. On the other hand, because the reflectance of position 5 is the smallest of all, the color difference value for that position is the highest owing to the high relative error in the synthesized reflectance. Overall, the color difference values listed in Tables 1 and 2 are quite small. These results verify the color accuracy of the prediction with use of the geometric coefficients developed in this study.

In addition to color difference, the estimation of the spectral variation in Eq. (32) is useful in evaluating the accuracy of the geometric coefficients. From Table 3 it is clear that the expectation for the plastic material is smaller than that for the fabric material, which indicates that the geometric description is more accurate for the plastic. When the probability of the reflectance for synthesis is equally likely in the range  $[0, 1]$ , the mean reflectance is 0.5. From Table 3 the variation of the synthesized reflectance caused by different  $(a_i, b_i)$  pairs is expected to be lower than 2% in most cases. It should also be noted that the expectation is the maximum value,

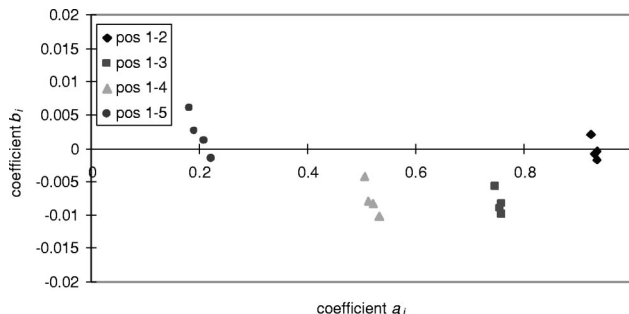


Fig. 6. Distribution of the geometric coefficient  $(a_i, b_i)$  pairs for the plastic cups.

**Table 1. Color Difference  $\Delta E_{CMC(1:1)}^*$  between Synthesized and Measured Reflectance with Use of Different  $(a_i, b_i)$  Pairs for the Four Plastic Cups<sup>a</sup>**

Position	Color Difference $\Delta E_{CMC(1:1)}^*$			
	First Pair	Second Pair	Third Pair	Fourth Pair
1-2	0.066	0.219	0.106	0.107
1-3	0.132	0.239	0.135	0.158
1-4	0.226	0.329	0.250	0.475
1-5	0.437	0.456	1.043	1.752

<sup>a</sup>The first  $(a, b)$  pair were calculated from the blue cup and the second, third, and fourth pairs from the green, red, and yellow cups, respectively.

**Table 2. Color Difference  $\Delta E_{CMC(1:1)}^*$  between Synthesized and Measured Reflectance with Use of Different  $(a_i, b_i)$  Pairs for the Three Fabrics**

Position	Color Difference $\Delta E_{CMC(1:1)}^*$		
	First Pair	Second Pair	Third Pair
1-2	0.269	0.601	0.335
1-3	0.294	1.035	0.302
1-4	0.398	1.210	0.501
1-5	0.915	2.280	1.706

**Table 3. Estimated Reflectance Difference  $E$  for Two Types of Materials**

Material	Estimated Reflectance Difference			
	Position 1-2	Position 1-3	Position 1-4	Position 1-5
Plastic	0.0025	0.0030	0.0063	0.0094
Fabric	0.0068	0.0105	0.0080	0.0104

which does not consider the negative correlation of  $a_i$  and  $b_i$ . Therefore the estimation can be approximately regarded as the upper limit of the spectral deviation, and the actual reflectance difference caused by the variation of different geometric coefficient pairs is always smaller than the estimated one.

The analysis of the geometric coefficient and error distribution can also be analyzed in the RGB color space of the camera output (Fig. 7). In the calculation of  $(A, B)$ , the reference  $V_k^x$  was arbitrarily selected from the pixels with medium saturations and intensities. Generally, those pixels are always in the nonshaded area of the surface and do not have much surface reflection. It is noted that diffuse reflection is recorded mainly by coefficient  $A$  [Fig. 7(b)] and that the surface reflection is recorded mainly by coefficient  $B$  [Fig. 7(c)]. Since the surrounding background of the image is almost gray, which is quite different from the object color, its geometric information is also recorded mainly by coefficient  $B$ . The average residual error [Fig. 7(d)] of the dichromatic reflection model fitting for the plastic cup is only 0.27 in the scale of

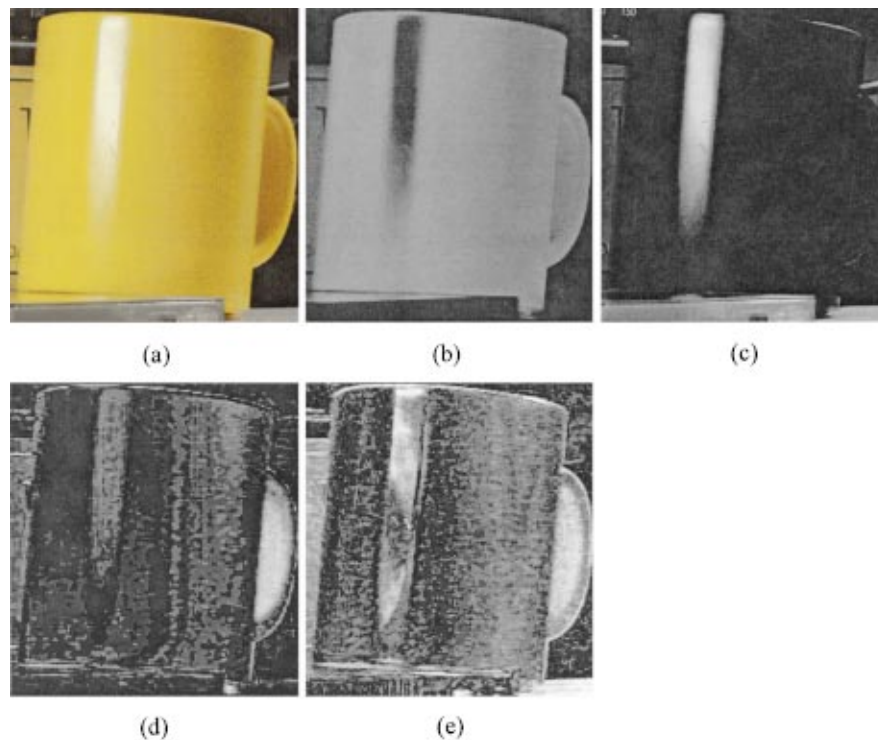


Fig. 7. Calculation of the geometric coefficient ( $A$ ,  $B$ ) from an image. (a) An image of a plastic cup, (b) coefficient  $A$ , (c) coefficient  $B$ , (d) residual error, (e) estimated coefficient variation calculated from four plastic cups of same size but of different colors. Note that images (b)–(e) were arbitrarily scaled for display.

[0, 255]. Four ( $A_i$ ,  $B_i$ ) pairs were calculated from four plastic cups with different colors, and the average pixel-wise estimated RGB color difference caused by the coefficient variation was  $\sim 6.0$ . It was noted that in addition to the geometric factor, the nonlinearity of the camera might contribute to this variation. It was found that the color differences caused by coefficient variation were larger in the region of highlight and cup handle than those in the other regions. This is expectable since the highlight is much more sensitive to the change of geometry. On the other hand, as the plastic cup is not completely opaque, there was a trace of light transmitting through the cup surface near the cup handle, causing a slight hue shift, which was not taken into account in the dichromatic reflection model.

After calculation of the geometric coefficient ( $A$ ,  $B$ ) from Fig. 7(a), new objects can be synthesized by providing a single target color (Fig. 8). In the color synthesis, a target color for mapping was obtained at the point on the target object surface that corresponded to that of the reference object. From Fig. 8 it is found that the synthesized images are perceptually very close to their corresponding target images in Fig. 8. Figure 9 is an example of fabric synthesis under the same illumination. The similarity between the synthesized images and the target images indicates that the dichromatic reflection model can also be used for certain textile fabrics.

Figure 10 is an example of color synthesis of fabrics with complicated draping under different illumination conditions. The original red fabric image was taken under a combination illumination of daylight and tungsten light, and the target blue fabric image was taken under

daylight. It is found that despite the different draping shapes, the color appearance of the synthesized image [Fig. 10(b)] is very similar to that of the target image. However, it can be seen that the synthesized colors in deep folds may be less accurate, as the interreflections between neighboring parts of the surfaces were not considered in this study. The light entering the folds of the object surface may be bounced several times before coming out. As the light is selectively reflected by the surface in each bounce, its spectrum is not the same as that of the light source for the subsequent bounces. Therefore the proposed algorithm may fail to describe this portion of the colors.

The proposed method for color synthesis performs quite well for materials with approximately similar reflection characteristics. It was found that the variation of the geometric coefficients was very small for polyester/cotton fabrics with different blend ratios. However, the method will fail to produce realistic synthesis results for materials with quite different reflection characteristics. For instance, the geometric coefficients obtained from cotton fabrics could not be directly used for the synthesis of satin fabrics.

It was also of interest to compare the performance of the proposed algorithm with the currently available technology such as color transfer.<sup>16</sup> In the color transfer method, the RGB image was first converted to the decorrelated  $l\alpha\beta$  color space. The  $l\alpha\beta$  was developed to minimize the correlation among the three channels so that the changes made in one color channel should minimally affect values in the other channels. The  $l\alpha\beta$  values for each pixel were then subtracted by the mean  $l\alpha\beta$  of the



Fig. 8. Synthesized images (top) and their corresponding target images (bottom) under the same illumination, where the geometric coefficient ( $A, B$ ) for synthesis is the same as that in Fig. 7. (Figures 8–11 may be found at the website <http://www.acad.polyu.edu.hk/~tcxinjh/research/publications.htm>.)

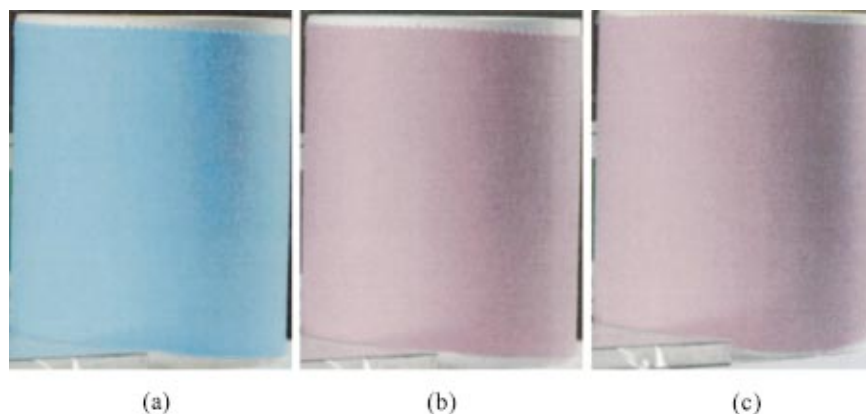


Fig. 9. Color synthesis for fabrics under the same illumination condition. (a) Original blue fabric image, (b) synthesized purple fabric image, (c) target purple fabric image.

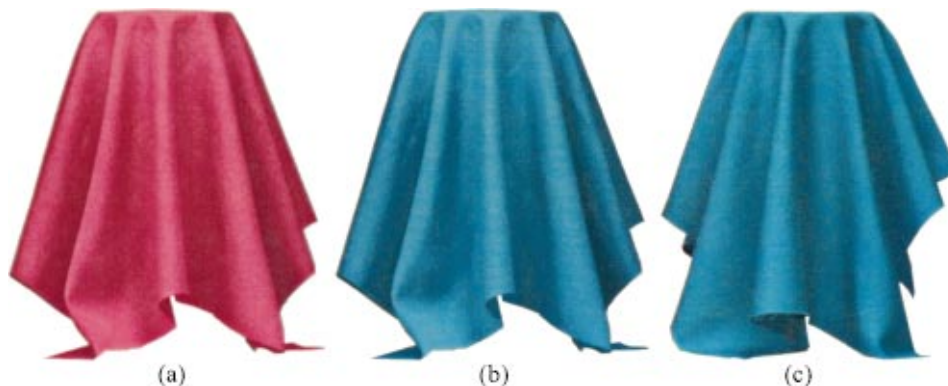


Fig. 10. Color synthesis for draping fabric under different illuminations. (a) Original red fabric image under the first illumination, (b) synthesized blue fabric image under the second illumination, (c) target blue fabric image under the second illumination.

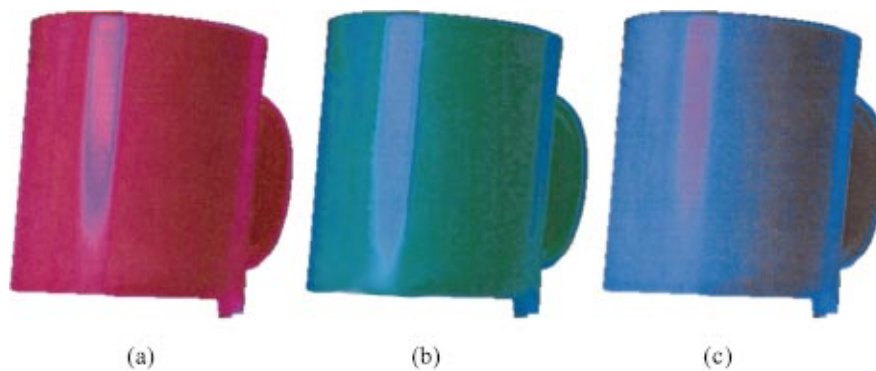


Fig. 11. Color synthesis of (a) red, (b) green, and (c) blue plastic cups by the color transfer method. The target images were the same as those in Fig. 8.

image, followed by the addition of the desired color. Finally, the modified  $l\alpha\beta$  values were converted back to RGB space. Color synthesis results of the plastic cups with the color transfer method are shown in Fig. 11. The target images were the same as those in Fig. 8. Because the color transfer method was based on the statistical distribution of color information, the background was manually removed during the color synthesis. In addition, in order not to bias the color transfer algorithm, the mean colors of the original and the target images were calculated in the areas without obvious highlights. It is clear from Fig. 11 that the simulation results of the color transfer method were very poor for color synthesis of 3D objects, especially in the highlight areas.

## 5. CONCLUSION

In this study a technique of accurate color synthesis of three-dimensional objects in an image was proposed. Given an original image, new images could be synthesized with any target colors by this technique, and the appearance of the synthesized images were perceptually very close to the actual images. Because the recovery of the explicit geometric information from an image is almost impossible, this study concentrated on the recovery of the implicit geometric information that was necessary and accurate for color rendering. This implicit information was calculated according to the dichromatic reflection model. Two types of materials, plastic and textile fabric, were investigated. It was found that the geometric coefficient pairs calculated from different objects made of similar materials were not the same; but they were negatively correlated, so the color difference produced by the different coefficient was small. The color synthesis method developed in this study represents an important step toward improvement of color fidelity in the virtual design, manufacturing, and retailing of products, especially for non-rigid products such as clothing. We note, however, that the synthesized color in deep folds of object surfaces may be less accurate as a result of interreflection. A detailed investigation of interreflection in color synthesis is beyond the scope of this paper, but we intend to study it in the future.

## ACKNOWLEDGMENT

The authors acknowledge financial support of this project from the Hong Kong Polytechnic University.

Corresponding author H.-L. Shen can be reached by e-mail at tcshenhl@polyu.edu.hk.

## REFERENCES

1. F. E. Nicodemus, J. C. Richmond, J. J. Hsia, I. W. Ginsberg, and T. Limperis, "Geometric considerations and nomenclature for reflectance," Monograph 160 (National Institute of Standards and Technology, Rockville, Md., 1997).
2. B. T. Phong, "Illumination for computer generated images," *Commun. ACM* **18**, 311–317 (1975).
3. J. F. Blinn, "Models of light refraction for computer synthesized pictures," *Comput. Graph.* **11**, 192–198 (1977).
4. K. E. Torrance and E. M. Sparrow, "Theory for off-specular reflection from roughened surface," *J. Opt. Soc. Am.* **57**, 1105–1114 (1967).
5. S. R. Marscher, S. H. Westin, E. P. F. Lafortune, and K. E. Torrance, "Image-based bidirectional reflectance distribution function measurement," *Appl. Opt.* **39**, 2592–2600 (2000).
6. G. J. Ward, "Measuring and modeling anisotropic reflection," *Comput. Graph.* **26**, 265–272 (1992).
7. K. J. Dana, B. Ginneken, S. K. Nayar, and J. J. Koenderink, "Reflectance and texture of real world surfaces," *ACM Trans. Graphics* **18**, 1–34 (1999).
8. H. B. Westlund and G. W. Meyer, "A BRDF database employing the Beard–Maxwell reflection model," in *Graphics Interface 2002* (Canadian Human-Computer Communications Society, Mississauga, Ontario, Canada, 2002), pp. 189–200.
9. L. B. Wolff, S. A. Shafer, and G. E. Healey, *Physics-Based Vision Principles and Practice: Shape Recovery* (Jones & Bartlett, Boston, Mass., 1992).
10. S. A. Shafer, "Using color to separate reflection components," *Color Res. Appl.* **10**, 210–218 (1985).
11. G. Healey, "Using color for geometry-insensitive segmentation," *J. Opt. Soc. Am. A* **6**, 920–937 (1989).
12. H. C. Lee, E. J. Breneman, and C. P. Schulte, "Modeling light reflection for computer vision," *IEEE Trans. Pattern Anal. Mach. Intell.* **12**, 402–409 (1990).
13. S. Tominaga, "Dichromatic reflection model for a variety of materials," *Color Res. Appl.* **19**, 277–285 (1994).
14. S. Tominaga, "Dichromatic reflection models for rendering object surfaces," *J. Imaging Sci. Technol.* **40**, 549–555 (1996).
15. H. L. Shen and J. H. Xin, "Dichromatic based rendering of texture images with high color fidelity," *J. Imaging Sci. Technol.* (to be published).

16. E. Reinhard, M. Ashikhmin, B. Gooch, and P. Shirley, "Color transfer between images," *IEEE Comput. Graphics Appl.* **21**, 34–41 (2001).
17. L. Peng, "Dichromatic based photographic modification," in *Proceedings of the Sixth Color Imaging Conference* (Society for Imaging Science and Technology, Springfield, Va., 1998), pp. 96–99.
18. L. Liu and G. Xu, "Color change method based on dichromatic reflection model," *Proceedings of International Conference on Signal Processing* (Institute of Electrical and Electronics Engineers, New York, 1996), pp. 1246–1249.
19. B. K. P. Horn and R. W. Sjöberg, "Calculating the reflectance map," *Appl. Opt.* **18**, 1770–1779 (1979).
20. K. Barnard and B. Funt, "Camera characterization for color research," *Color Res. Appl.* **27**, 152–163 (2002).
21. F. J. Clarke, R. McDonald, and R. Rigg, "Modification to the JPC79 color difference formula," *J. Soc. Dyers Colorists* **100**, 117–148 (1984).